2.2. CARBON DIOXIDE

2.2.1. IN SITU CARBON DIOXIDE MEASUREMENTS

The mole fraction of atmospheric CO_2 was measured with continuously operating non-dispersive infrared (NDIR) analyzers at the four CMDL observatories during 2000 and 2001, as in previous years. Monthly and annual mean CO_2 concentrations are given in Table 2.2. These values are provisional, pending final calibrations of reference gas standards. Preliminary selected hourly average CO_2 mole fractions for 2000 and 2001 are plotted for the four observatories in Figure 2.1.

Except at the South Pole Observatory (SPO), the CO_2 in situ analyzers performed without any major problems. At SPO, the Siemens Ultramat 5F CO_2 analyzer experienced some mechanical problems in March 2000. An incandescent light bulb that is used to detect the rotational speed of the chopper wheel inside the analyzer burned out. A replacement bulb, not of the original type, was installed to allow the analyzer to continue working. However, this change resulted in a change in the characteristics of the analyzer, such as reduced sensitivity and reduced output. Although the measurements resulting from the analyzer appeared to be normal, further inspection of the data showed some small offsets on the order of several tenths of a part per million (ppm) compared with flask data taken at SPO. There was also evidence of changes in the analyzer characteristics whenever the output signal of the analyzer was modified. This can be seen in December 2000 when a shift in the data of about 0.5 ppm occurred after the analyzer output was shifted upward. The analyzer was replaced on February 14, 2001, with a LI-COR Model 6251 CO_2 analyzer. Until the old Siemens analyzer can be returned to the CMDL Boulder laboratory for testing, and until all reference gases used in 2000 and 2001 are returned, the data from SPO must be considered very preliminary and subject to change.

2.2.2. FLASK SAMPLE CARBON DIOXIDE MEASUREMENTS

The CMDL Global Cooperative Air Sampling Network (Figure 2.2) is the most extensive and representative network in existence for the measurement of climatically important trace gases. Samples are currently collected approximately weekly at 47 fixed locations. The samples are measured at CMDL for CO_2, CH_4, CO, H_2, N_2O, and SF_6, and at INSTAAR for ^{13}C and [18]O of CO_2. In 2000, 7400 samples were analyzed, and in 2001, 7000 were analyzed. Samples from seven sites are measured for ^{13}C of

TABLE 2.2. Provisional 2000 and 2001 Monthly and Annual Mean CO_2 Mole Fractions from Continuous Analyzer Data (μmol mol^{-1}, Relative to Dry Air), for the Four CMDL Observatories

Month	BRW	MLO	SMO	SPO
2000				
Jan.	374.76	369.05	368.39	366.36
Feb.	376.48	369.34	368.20	366.21
March	374.54	370.35	368.60	366.15
April	375.42	371.77	368.02	366.22
May	375.88	371.32	367.64	366.35
June	372.34	371.53	367.37	366.69
July	365.98	369.75	368.16	367.15
Aug.	360.77	368.20	368.36	367.63
Sept.	363.07	366.86	368.07	367.84
Oct.	368.62	366.94	368.73	367.84
Nov.	370.97	368.28	369.06	367.75
Dec.	373.03	369.62	368.99	367.99
Year	370.99	369.42	368.30	367.01
2001				
Jan.	375.64	370.46	369.42	367.83
Feb.	376.36	371.44	369.80	367.54
March	376.29	372.38	369.78	367.48
April	377.41	373.33	369.30	367.75
May	377.49	373.78	368.41	368.01
June	375.27	373.09	369.73	368.26
July	367.71	371.51	370.30	368.69
Aug.	361.05	369.48	369.93	369.19
Sept.	363.58	368.12	369.97	369.47
Oct.	368.81	368.59	370.08	369.71
Nov.	373.94	369.74	370.24	369.77
Dec.	376.19	371.10	370.51	369.58
Year	372.48	371.08	369.79	368.61

μmol mol^{-1} is abbreviated as ppm.

CH_4 at INSTAAR; samples from three sites are measured for [17]O of CO_2 at the University of California at San Diego; and samples from one site are measured for [2]H (deuterium) in H_2 at the California Institute of Technology. The mole fraction and isotopic measurements are used to quantify global and regional carbon budgets by inverse techniques or to constrain source/sink estimates obtained from process-based models.

Several changes to the network occurred during 2000-2001. Sampling began at Moody, Texas (WKT), in 2001 as part of the new tall-tower project there. After resumption of
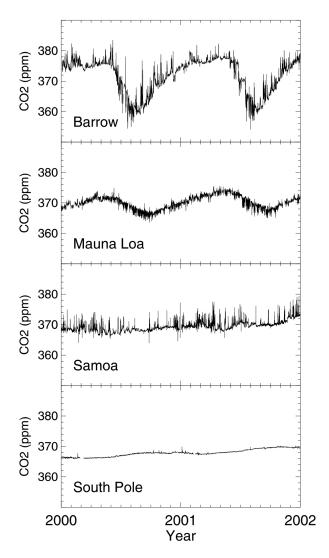
Fig. 2.1. Hourly mean CO_2 mole fractions in dry air, expressed in μmol mol^{-1} (ppm, parts per million) measured at the four CMDL observatories during 2000 and 2001. Data were not selected for background conditions. Only hours with instrument malfunctions were omitted.

regular sampling at Christmas Island (CHR) in 1998, logistical problems again interrupted sampling in 2001. Resumption of sampling at CHR or another island (Palmyra) in the region is planned. Sampling was discontinued at the Kaashidhoo Climate Observatory (KCO) when the observatory closed; Gozo, Malta, was discontinued due to lack of sampling; and the WITN tall-tower site in Grifton, North Carolina (ITN), was discontinued when the tower project there ended.

The last CCGG shipboard sampling program in the Pacific Ocean ended when the *Argentina Star* completed its route in 2001. Although modeling studies have shown the importance of the data obtained from the Pacific Ocean and the previously interrupted South China Sea cruises, these programs could not be continued.

One component of the ongoing effort to assure the quality of the flask network data is the measurement each analysis day of test flasks filled with air of known composition. The test-flask CO_2 results for 1998-2001 are plotted in Figure 2.3a. The symbols represent the difference between the measured value of each flask and the value assigned to the high-pressure cylinder from which the flasks are filled. The larger scatter observed prior to 1999 (asterisks) was reduced in early 1999 when a new person started filling the test flasks. Since that change, careful adherence to the filling procedure has produced a test-flask record (plus symbols) that can be used to investigate instrument performance and sources of uncertainty in the CO_2 measurements.

The red curve in Figure 2.3a is a smooth fit to the data, showing significant long-term variations in the test-flask differences. One possible explanation of these long-term variations is that the CO_2 mole fractions of the flask analysis reference gases are changing over time. The black lines in Figure 2.3a show the drifts in the flask analysis reference gases relative to their initial assigned values determined by periodic recalibrations during their lifetimes. Test-flask differences based on data corrected for reference gas drifts are plotted in Figure 2.3b. Much less long-term signal is seen in the drift-corrected results. The standard deviation of the test-flask differences is 0.08 ppm, which is a good approximation of the analytical precision of an individual flask measurement. This value is the sum of several sources of imprecision. The uncertainty arising from the high-frequency (1-Hz) noise of the NDIR instrument is ~0.02 ppm (1 standard error of the 30-s average). Additional lower frequency noise is observed in the variability of the three reference gases used to calibrate the instrument several times during each analysis day. The red squares in Figure 2.3b represent the difference between the value assigned to the mid reference gas and the value calculated (linearly) for mid using the high and low reference gases. The offset from zero is due to the instrument nonlinearity (which is accounted for in the determination of actual flask values), and the variability is measurement noise resulting from pressure and temperature variations, and possible regulator or other gas-handling effects, which are not accounted for by the calibration scheme. This source contributes 0.04 ppm to the overall imprecision. Based on this analysis, the remaining 0.07 ppm (uncertainties are summed in quadrature) of the test-flask imprecision likely occurs during the filling of the test flasks or results from interaction of the test gas with the flask between filling and analysis.

During 1999 and 2000 there was no significant offset in the test-flask measurements. In 2001 there is an as-yet-unexplained offset of ~0.05 ppm. Reliable test-flask data, as shown in Figure 2.3b, are useful in the interpretation of results from interlaboratory flask intercomparison experiments (discussed in section 2.7). The stability of the CMDL CO_2 analytical apparatus demonstrated by the test flasks makes it hard to postulate a CMDL analytical problem as the cause for the significant differences observed when CMDL and the Meteorological Service of Canada (MSC) measure air from the same flasks.

The 2000 and 2001 annual mean CO_2 mole fractions (mixing ratios) calculated from smooth curves fitted to the
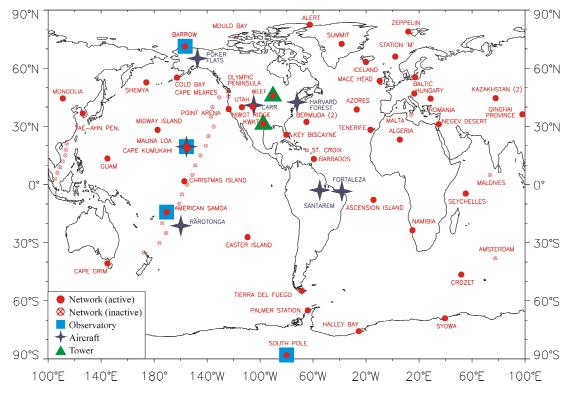
Fig. 2.2. Locations of the CCGG measurement programs, including the baseline observatories (squares), Global Cooperative Air Sampling Network (circles), discontinued sites of same (open circles with cross), aircraft vertical profiles (stars), and the very tall tower sites (triangles).

data for 47 sites in the CMDL/CCGG Global Cooperative Air Sampling Network are given in Table 2.3. The globally averaged CO_2 mole fraction and long-term trend (seasonal cycle filtered out) are shown as smooth curves in Figure 2.4a. In 2001 the globally averaged CO_2 mole fraction was 370.2 compared with the pre-industrial value of ~280 ppm in 1880. The CO_2 increase from 1999 to 2001 was 1.35 ppm yr^{-1}, slightly lower than the 1979-2001 average growth rate of 1.5 ppm yr^{-1} and about half of the 1997-1998 increase of 2.7 ppm yr^{-1}. The globally averaged CO_2 growth rate as a function of time is shown in Figure 2.4b.

2.2.3. CARBON DIOXIDE STANDARDS AND REFERENCE GAS CALIBRATIONS

The 15 primary WMO standards, ranging in CO_2 mole fraction from approximately 250 to 520 µmol mol^{-1}, were calibrated at regular intervals of slightly more than 1 year by CMDL's manometric system [*Zhao et al.,* 1997]. The function of the primary standards is to provide continuity to the WMO scale, as well as a quality control check on the performance of the manometric system. From September 1996 through August 2001, 237 individual manometric determinations were made of the CO_2 mole fractions in these cylinders. The results of the analyses are summarized in Table 2.4. For comparison, the CO_2 mole fractions

measured by the Scripps Institution of Oceanography (SIO) by infrared absorption relative to the WMO X93 mole fraction scale, maintained by SIO, are also shown in Table 2.4. The mean precision of an individual manometric measurement by CMDL, indicated in Table 2.4 as the standard deviation, has been about 1 part in 3200. The mole fractions analyzed by CMDL are lower than by SIO at the low end of the scale and higher at the high end, while in the atmospheric CO_2 concentration range of 340 to 400 µmol mol^{-1} SIO is on average 0.10 µmol mol^{-1} less than CMDL. To maintain and propagate the WMO scale, the assigned values of the WMO primary standards have been based on both the SIO and CMDL measured values. The assigned values as of January 2000 are indicated in Table 2.4 as "old scale." Contrary to plans described in the previous CMDL report [*Tans et al.*, 2001], it was decided to wait a bit longer before basing the assignments of the WMO primary standards on the CMDL manometric measurements alone. CMDL recently received from SIO revisions of its earlier reported IR measurements of the WMO primary standards (not incorporated in Table 2.4), and an assessment and revision of the WMO scale, to be named X2002, will be described in detail in a future publication.

Because the goal is to maximize the useful life span of the primary standards, the primary calibration scale is transferred via NDIR measurements, approximately twice a
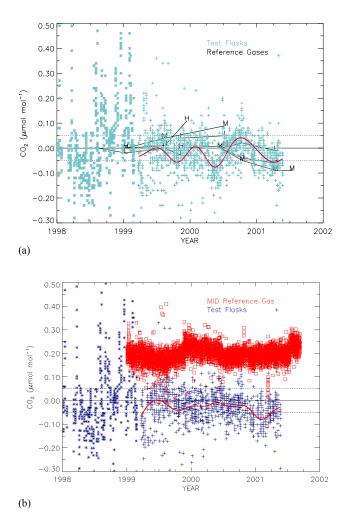
(a)

(b)

Fig. 2.3. (a) Comparison of the measurements of test flasks filled from cylinders having well-calibrated concentrations with the assigned concentration of those cylinders. Drifts of high, mid, and low (H, M, and L) reference gases are used in the measurements of the test flasks (and all other flasks). The red curves are smooth fits to the test-flask data. (b) Same as (a) after correction for drift of H, M, and L. Squares are the measured values of reference cylinder M based on linear interpolation of measurements of H and L, plotted as the difference from the assigned value of M.

year, to a set of secondary standards. The secondary standards, which typically have a useful lifespan of 3 to 4 years, are in turn used to calibrate all other cylinders, in which each cylinder is always compared with a set of four bracketing secondary standards. During 2001 about 600 cylinders were assigned a value on the WMO Mole Fraction Scale in this way. The reproducibility, in the range between 250 and 520 $\mu mol\ mol^{-1}$, has generally been better than 0.05 $\mu mol\ mol^{-1}$. In the range of 325-425 $\mu mol\ mol^{-1}$, the reproducibility (1σ) has been 0.014 $\mu mol\ mol^{-1}$ [*Kitzis and Zhao*, 1999].

On request, calibrations can be performed with the manometric system well outside of the range of atmospheric

CO_2 values. Because there has been some demand for calibrations well above 520 $\mu mol\ mol^{-1}$, new primary CO_2 standards were created at the high end of the range, at approximately 600, 700, 1000, 1500, 2000, 2500, and 3000 $\mu mol\ mol^{-1}$. The standards will allow CO_2 calibrations to be performed by the comparative infrared absorption technique rather than the time-consuming manometric determinations.

Cylinders prepared by CMDL with a specified CO_2 concentration undergo the following procedures at its clean-air pumping station at high elevation on Niwot Ridge, 30 km west of Boulder:

New or recently hydrotested cylinder: (1) The cylinder is vented and then pressurized twice with dry natural air to about 20 atm (300 psi) and vented again. (2) The cylinder is filled to about 34 atm (510 psi) with dry natural air and stored for several weeks. (3) Before the final fill, the cylinder is first vented and then spiked with either 10% or zero CO_2-in-air, depending on the desired final mixing ratio. (4) The final fill is made with ambient and dried natural air to 135 atm (2000 psi), during which the ambient CO_2 mixing ratio is monitored. (5) The water vapor content of the filled cylinder is measured; it must be less than 5 ppm and is usually less than 1 ppm. Drying is accomplished with magnesium perchlorate, $Mg(ClO_4)_2$. The pump is a RIX oil-less diving compressor.

Previously used cylinder: Steps 1 and 2 are replaced by one vent and one fill with dry natural air to a pressure of 20 atm. Other trace gases, such as CH_4 and CO, can be targeted to specified values in the same cylinders.

2.2.4. MEASUREMENTS OF STABLE ISOTOPES OF ATMOSPHERIC CO_2

The Stable Isotope Laboratory (SIL) at the Institute of Arctic and Alpine Research at the University of Colorado has, for the past decade, worked closely with CCGG to measure stable isotope ratios of atmospheric greenhouse gases. Currently $\delta^{13}C$ and $\delta^{18}O$ of atmospheric CO_2 are measured in nearly all of the NOAA Global Cooperative Air Sampling Network, including flask sites, tall towers, and aircraft. Samples from 13 sites are also analyzed for $\delta^{13}C$ of atmospheric CH_4, with plans to expand this measurement to the full network when funding permits. A system to measure δD in atmospheric CH_4, as well as isotopes in water vapor extracted from the NOAA flasks, is also in the testing phase. Planned future analyses include isotopes of atmospheric CO and N_2O.

$\delta^{13}C$ of Atmospheric CO_2

A current "flying carpet" plot of $\delta^{13}C$ of CO_2 is shown in Figure 2.5. These data are key to the separation of fluxes of atmospheric CO_2 between the terrestrial biosphere and the ocean. Plants discriminate against $^{13}CO_2$ during photo-synthesis by about −18 per mil (‰). This is a relatively large effect compared with the few-per-mil fractionation that occurs when CO_2 goes into and out of the surface ocean. A reconstruction of net terrestrial biospheric and oceanic fluxes is shown in Figure 2.6 from the CCGG two-dimensional (latitude, height) transport model [*Tans et al.*, 1989]. Several key observations can be made from this figure. The temperate latitudes of the northern hemisphere,

TABLE 2.3. Provisional 2000 and 2001 Annual Mean Mixing and Isotopic Ratios
from the Global Cooperative Air Sampling Network

Site Code	Location	CO$_2$ (μmol mol^{-1}) 2000	2001	CH$_4$ (nmol mol^{-1}) 2000	2001	CO (nmol mol^{-1}) 2000	2001	N$_2$O (nmol mol^{-1}) 2000	2001	SF$_6$ (pmol mol^{-1}) 2000	2001	δ^{13}CO$_2$ (‰) 2000	2001	δ^{13}CH$_4$ (‰) 2000	2001
ALT	Alert, Nunavut, Canada	370.6	372.0	1829.0	1829.7	126.1	124.8	315.5	316.2	4.44	4.64	-8.20	-8.18	[ ]	-47.47
ASC	Ascension Island	367.8	369.6	1717.2	1714.3	72.1	67.0	315.0	315.7	4.38	4.59	-7.98	-7.97	[ ]	[ ]
ASK	Assekrem, Algeria	369.8	371.4	1779.3	1779.7	102.9	103.3	315.8	316.6	4.57	4.77	-8.09	-8.09	[ ]	[ ]
AZR	Terceira Island, Azores	369.9	[ ]	1801.8	[ ]	111.6	[ ]	315.7	[ ]	4.63	[ ]	-8.08	[ ]	[ ]	[ ]
BAL	Baltic Sea	374.6	[ ]	1861.3	[ ]	176.9	[ ]	316.5	[ ]	4.75	[ ]	-8.35	[ ]	[ ]	[ ]
BME	Bermuda (east coast)	370.6	371.6	1799.6	1796.0	119.3	118.2	315.8	316.4	4.65	4.83	-8.20	-8.13	[ ]	[ ]
BMW	Bermuda (west coast)	370.5	371.7	1806.8	1798.6	125.3	118.1	315.8	316.4	4.65	4.85	-8.15	-8.16	[ ]	[ ]
BRW	Barrow, Alaska	370.8	372.2	1840.8	1837.6	125.4	126.7	315.2	315.9	4.63	4.82	-8.22	-8.18	-47.43	-47.53
BSC	Black Sea, Romania	377.7	377.7	1905.1	1909.0	239.3	233.1	316.7	317.3	4.70	4.87	-8.46	-8.39	[ ]	[ ]
CBA	Cold Bay, Alaska	[ ]	372.1	1825.6	1826.4	125.3	125.2	315.8	316.2	4.64	4.82	-8.33	-8.20	[ ]	[ ]
CGO	Cape Grim, Tasmania	366.9	368.5	1708.1	1706.2	49.1	48.7	314.3	314.9	4.34	4.54	-7.97	-7.95	-46.94	[ ]
CHR	Christmas Island, Kiribati	370.0	[ ]	1736.0	[ ]	74.6	[ ]	315.9	[ ]	4.45	[ ]	-7.99	[ ]	[ ]	[ ]
CRZ	Crozet Island	366.8	[ ]	1706.3	[ ]	51.4	[ ]	314.4	[ ]	4.33	[ ]	-8.00	[ ]	[ ]	[ ]
EIC	Easter Island	366.2	368.1	1708.1	1705.4	59.4	64.2	314.7	315.1	4.36	4.54	-7.95	-7.87	[ ]	[ ]
GMI	Mariana Islands, Guam	369.3	371.0	1753.9	1756.1	78.9	88.3	315.7	316.4	4.51	4.72	-8.03	-8.04	[ ]	[ ]
HBA	Halley Bay, Antarctica	366.7	[ ]	1706.2	[ ]	49.2	[ ]	314.1	[ ]	4.32	[ ]	-7.98	[ ]	[ ]	[ ]
HUN	Hegyhatsal, Hungary	374.2	[ ]	1872.8	[ ]	194.8	[ ]	316.9	[ ]	4.79	[ ]	-8.30	[ ]	[ ]	[ ]
ICE	Heimaey, Iceland	370.1	371.7	1824.6	1828.5	121.5	125.7	315.7	316.4	4.64	4.84	-8.17	-8.19	[ ]	[ ]
IZO	Izaña Obs., Tenerife	370.2	371.7	1782.2	1780.0	99.8	101.8	315.8	316.4	4.58	4.77	-8.08	-8.12	[ ]	[ ]
KEY	Key Biscayne, Florida	371.2	373.2	1794.0	1789.0	112.6	111.1	315.8	316.5	4.62	4.80	-8.10	-8.16	[ ]	[ ]
KUM	Cape Kumukahi, Hawaii	369.9	371.4	1775.2	1776.0	94.6	100.6	315.7	316.4	4.57	4.77	-8.07	-8.08	-47.16	-47.53
KZD	Sary Taukum, Kazakhstan	371.5	373.3	1845.1	1845.3	146.7	[ ]	316.0	316.5	4.64	4.83	-8.23	-8.23	[ ]	[ ]
KZM	Plateau Assy, Kazakhstan	369.1	371.2	1816.4	1816.2	131.5	127.4	315.9	316.5	4.62	4.81	-8.06	-8.14	[ ]	[ ]
LEF	Park Falls, Wisconsin	373.1	374.4	1865.8	1856.5	143.4	142.3	315.9	316.4	4.71	4.85	-8.30	-8.24	[ ]	[ ]
MHD	Mace Head, Ireland	370.0	371.8	1820.2	1819.8	120.9	128.4	314.3	315.7	4.65	4.86	-8.12	-8.12	[ ]	[ ]
MID	Sand Island, Midway	369.5	371.5	1786.2	1788.4	105.0	109.1	315.7	316.3	4.59	4.80	-8.08	-8.08	[ ]	[ ]
MLO	Mauna Loa, Hawaii	369.6	371.2	1762.9	1764.3	89.2	93.4	315.7	316.3	4.52	4.73	-8.06	-8.06	-47.09	-47.20
NMB	Gobabeb, Namibia	[ ]	[ ]	[ ]	[ ]	[ ]	[ ]	[ ]	[ ]	[ ]	[ ]	[ ]	[ ]	[ ]	[ ]
NWR	Niwot Ridge, Colorado	370.3	372.4	1790.1	1793.9	111.2	119.2	315.7	316.3	4.60	4.79	-8.10	-8.13	-47.14	-47.23
PSA	Palmer Station, Antarctica	366.9	368.6	1707.2	1706.3	47.3	48.3	314.5	315.0	4.32	4.52	-8.00	-8.00	[ ]	[ ]
PTA	Point Arena, California	[ ]	376.8	[ ]	1809.0	[ ]	126.3	[ ]	317.3	[ ]	4.85	[ ]	-8.42	[ ]	[ ]
RPB	Ragged Point, Barbados	369.1	371.2	1770.8	1767.0	91.9	93.0	315.7	316.4	4.56	4.75	-8.02	-8.01	[ ]	[ ]
SEY	Mahé Island, Seychelles	368.3	[ ]	1725.6	[ ]	77.9	[ ]	315.3	[ ]	4.41	[ ]	-7.98	[ ]	[ ]	[ ]
SHM	Shemya Island, Alaska	370.5	372.3	1824.2	1827.2	129.5	132.6	315.9	316.5	4.63	4.84	-8.20	-8.19	[ ]	[ ]
SMO	American Samoa	368.2	369.8	1714.5	1712.4	54.7	58.6	315.1	315.7	4.40	4.58	-7.95	-7.97	-47.02	-47.18
SPO	South Pole, Antarctica	366.8	368.6	1706.9	1705.8	45.9	48.4	314.2	314.8	4.33	4.52	-7.99	-8.00	-46.96	[ ]
STM	Ocean Station M	370.6	371.8	1828.6	1828.3	129.0	128.2	315.6	316.3	4.66	4.85	-8.18	-8.17	[ ]	[ ]
SUM	Summit, Greenland	[ ]	[ ]	[ ]	[ ]	[ ]	[ ]	[ ]	[ ]	[ ]	[ ]	[ ]	[ ]	[ ]	[ ]
SYO	Syowa Station, Antarctica	366.9	[ ]	1706.3	[ ]	46.7	[ ]	314.3	[ ]	4.32	[ ]	-8.00	[ ]	[ ]	[ ]
TAP	Tae-ahn Pen., Rep. of Korea	373.3	376.4	1855.7	1851.9	219.1	207.8	316.5	317.0	4.70	4.87	-8.31	-8.40	[ ]	-47.45
TDF	Tierra del Fuego, Argentina	366.8	[ ]	1707.5	[ ]	48.4	[ ]	314.5	[ ]	4.35	[ ]	-7.98	[ ]	[ ]	[ ]
UTA	Wendover, Utah	371.3	372.2	1799.2	1802.5	120.9	120.7	315.9	316.5	4.65	4.82	-8.17	-8.18	[ ]	[ ]
UUM	Ulaan Uul, Mongolia	371.2	372.4	1830.7	1829.7	148.9	154.6	315.9	316.4	4.64	4.84	-8.16	-8.16	[ ]	[ ]
WIS	Negev Desert, Israel	371.2	372.7	1827.0	1823.8	149.0	146.2	316.0	316.8	4.66	4.88	-8.17	-8.15	[ ]	[ ]
WLG	Mt. Waliguan, P.R. of China	370.3	[ ]	1807.8	[ ]	133.0	[ ]	315.9	[ ]	4.66	[ ]	-8.14	[ ]	[ ]	[ ]
WKT	Moody, Texas	[ ]	[ ]	[ ]	[ ]	[ ]	[ ]	[ ]	[ ]	[ ]	[ ]	[ ]	[ ]	[ ]	[ ]
ZEP	Ny-Ålesund, Svalbard	371.2	372.5	1831.4	1835.3	127.5	127.3	315.7	316.4	4.66	4.84	-8.20	-8.24	[ ]	[ ]

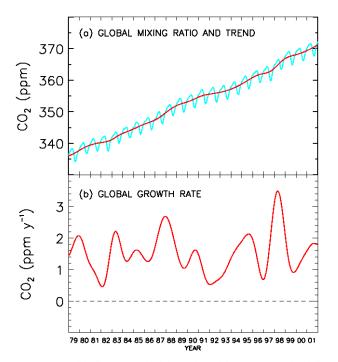Square brackets indicate insufficient data to calculate the annual mean.

Fig. 2.4. (a) Globally averaged mixing ratio and long-term trend and (b) growth rate of atmospheric CO_2 as measured by the CMDL Global Cooperative Air Sampling Network.

a land-dominated region, are always a sink of carbon for both ocean and land, with the land sink larger than the ocean sink. In the tropics, both land and ocean are almost always a source of carbon. The land source is over-estimated and the ocean source underestimated in this analysis because conversion of C-3 forests to C-4 pastures

is not included in the model. Plants with the C-3 photo-synthetic pathway (the majority of plants) discriminate against $^{13}CO_2$, whereas C-4 plant discrimination is much smaller and thus more oceanlike in its effect on isotopic ratios. When this land conversion effect is included, the net land curve will be near zero. Importantly, this implies that there must be a sink of CO_2 in the living tropical biosphere because deforestation is clearly contributing to a source of CO_2. The impact of land conversion on the isotope record is the subject of one of CCGG's recent publications [*Townsend et al.,* 2002].

A key challenge to keeping these data useful for the modeling community is maintaining a stable and precise isotopic scale over time. Measurement precision needs to be extremely high, at least ±0.01‰ (1σ), in order to keep the global uncertainty in the above deconvolutions to less than 0.5×10^{14} moles of carbon. This requires constant calibrations and the maintenance of a large suite of calibrated cylinders that are measured periodically to detect and distinguish between any observed instrument drift and possibly long-term change occurring in the suite of calibrated cylinders. In addition, the laboratory maintains several closely monitored intercomparison projects with other laboratories in which both laboratories analyze the same air-flask sample. Intercomparison projects are important because they can alert laboratories to analytical problems that can be addressed in near-real time. SIL also plays a key role along with laboratories in Japan, Australia, United States, and Germany in an ongoing effort to establish an international standard for isotopes in atmos-pheric greenhouse gases.

Spatial and Temporal Patterns of Terrestrial Discrimination

Measurements of CO_2 and $\delta^{13}C$ are used to deduce meridional patterns in oceanic and terrestrial CO_2 uptake in a simple two-dimensional inverse model. The input to the

TABLE 2.4. Summary of Measurements of the WMO Primary CO_2 Standards Expressed as $\mu mol\ mol^{-1}$ in Dry Air (ppm), September 1996-August 2001

Cylinder Serial Number	N	CMDL		SIO		Old Scale	Difference (mano − old)*
		(ppm)	(1σ)	(ppm)	(1σ)	(ppm)	(ppm)
110	12	246.68	0.10	246.82	0.52	246.78	−0.10
102	17	304.39	0.11	304.43	0.18	304.41	−0.02
111	19	324.01	0.15	324.04	0.13	324.03	−0.02
130	13	337.27	0.10	337.29	0.12	337.28	−0.01
121	11	349.39	0.08	349.35	0.12	349.36	0.03
103	18	353.35	0.10	353.18	0.12	353.24	0.11
139	14	360.90	0.06	360.82	0.14	360.84	0.06
105	16	369.38	0.12	369.32	0.16	369.34	0.04
136	15	381.34	0.12	381.24	0.17	381.26	0.08
146	15	389.54	0.11	389.47	0.20	389.49	0.05
101	17	396.35	0.15	396.17	0.20	396.22	0.13
106	13	412.09	0.14	411.91	0.25	411.96	0.13
123	15	423.06	0.16	422.88	0.29	422.93	0.13
107	21	453.13	0.19	452.76	0.40	452.90	0.23
132	21	521.39	0.16	520.99	0.80	521.10	0.29

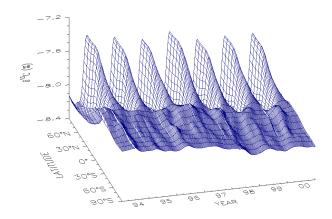*Difference between CMDL manometric values and values determined with the old scale.

Fig. 2.5. Three-dimensional representation of the latitudinal distribution of the carbon isotopic composition of atmospheric carbon dioxide in the marine boundary layer. The measurements of stable isotope ratios were made at the University of Colorado INSTAAR on air samples provided by the CMDL Global Cooperative Air Sampling Network. The surface represents data smoothed in time and latitude. The isotope data are expressed as deviations of the carbon-13/carbon-12 ratio in carbon dioxide from the VPDB-CO_2 standard in per mil (parts per thousand).
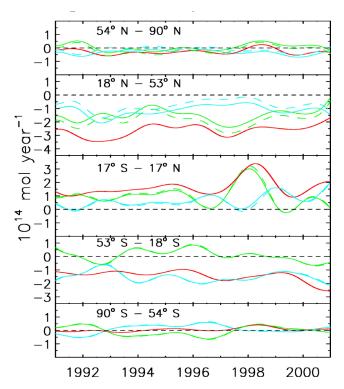

Fig. 2.6. Reconstructions of net CO_2 fluxes between the atmosphere and the terrestrial biosphere (green) and the ocean (blue) as well as the total net flux between the atmosphere and the Earth's surface from pCO_2 (red), in major latitude zones. Dashed lines represent source/sink reconstructions using values for terrestrial discrimination that are consistent with CCGG observations.

model is smoothed over time and does not include high-frequency variability that exists in the data. This allows correlation of the high-frequency variations in CO_2 and $\delta^{13}C$ in order to check model-derived patterns of surface discrimination. In a manner similar to that of *Bakwin et al.* [1998b], changes in CO_2 and $\delta^{13}C$ are related to isotopic discrimination of a source or sink using a time-varying background of CO_2 and $\delta^{13}C$. The observed CO_2 mole fraction is defined to be the sum of contributions from some regional background concentration and regional fluctuations due to biospheric sources and sinks and fossil fuel emissions. A similar equation is defined for ^{13}C using the product of CO_2 and $\delta^{13}C$, which, to a good approximation, is conserved [*Tans et al.,* 1993].

$$C = C_{bg} + C_{ff} + C_{bio} \; , \qquad (1)$$

$$\delta C = (\delta C)_{bg} + (\delta C)_{ff} + (\delta C)_{bio} \;\; , \qquad (2)$$

where C refers to CO_2 mole fraction and δ refers to $\delta^{13}C$. The subscript *bg* refers to background, *ff* to fossil fuel, and *bio* to terrestrial biological contribution. Terms with no subscript refer to the observed atmospheric values. For each sampling site, the data are fitted with a curve consisting of a second-order polynomial and two harmonic functions [*Thoning et al.*, 1989]. This "smooth curve" represents a regional average for either CO_2 or $\delta^{13}C \times CO_2$, so the background components in equations (1) and (2) are defined by the smooth-curve fits. Then, if the molar emission ratio (R) of CO to CO_2 for fossil fuels is known, C_{ff} can be determined according to equations (3) and (4):

$$CO = CO_{bg} + CO_{ff} \;\; , \qquad (3)$$

$$C_{ff} = (CO - CO_{bg})/R \; . \qquad (4)$$

As with CO_2, CO_{bg} is defined to be the smooth-curve fit to the CO data. With this model, changes in CO due to OH photochemistry and biomass burning are neglected. However, *Bakwin et al.* [1998b] showed that changes in CO:CO_2 emission ratios of 15% and the inclusion of OH consumption had very little effect on the calculation of δ_{bio}. A value for R of 20 ppb CO/ppm CO_2 is assumed. Values for δ_{ff} are taken from a zonally and annually averaged data set of $\delta^{13}C$ of fossil fuel emissions for 1992 [*Andres et al.*, 1996]. For a given site, values from the four nearest 1° zonal bands are averaged to calculate δ_{ff}. Equations (1), (2), and (4) are then combined to give equation (5):

$$(\delta C)^R - \delta_{ff} CO^R/R = \delta_{bio} \, (C^R - CO^R/R) \; . \qquad (5)$$

Superscript R denotes the residual difference between the data and smooth curve. The right-hand side of equation (5) is plotted against the left such that the slope of the line is δ_{bio}.

Figure 2.7 shows δ_{bio} for the subset of continental sites with more than 3 years of data available for May, June,

July, August, and September. Fluctuations in summertime data are more likely to be related to biospheric fluxes, and thus calculated discrimination values are less sensitive to the fossil fuel correction. Analysis was restricted to continental sites because they are the most likely to satisfy the assumptions implicit in equations (1)-(5). Specifically, the equations do not account for fluctuations about the smooth curve resulting from oceanic exchange processes. At the continental sites used here it is likely that most oceanic fluxes have been mixed into the atmosphere to the extent that they are captured by variations in the smooth curve, and the remaining fluctuations are mainly a result of terrestrial processes. Note that other sites, during certain times, may also satisfy the assumptions of equations (1)-(5).

δ_{bio} varies from about −30 to −24‰ (Figure 2.7). The average of the 14 sites used is −26.0 ± 1.9‰ (1σ between sites). When data from all continental sites are binned as one site, δ_{bio} = −24.5 ± 0.2‰. This second average is heavier than the first because sites with more data, and especially those with larger residuals, like the tall tower sites ITN, HUN, and LEF, are given more weight. These values of δ_{bio} correspond to isotopic discrimination values of 18.0 and 16.5‰, respectively, for the 14 sites and all continental sites.
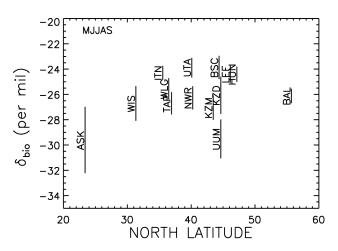

Fig. 2.7. Isotopic composition of biospheric sources at the continental stations of the CMDL Global Cooperative Air Sampling Network for May through September. Bars to the right of the symbols (site codes) denote estimated uncertainty.

Fung et al. [1997], using a Simple Biosphere Model (SiB2) coupled to a general circulation model (GCM), found that discrimination changed from 10 to 20‰ between 30° and 50°N. *Lloyd and Farquhar* [1994] used a different approach to calculate discrimination values ranging only between 15 and 16.5‰ over the same latitudes. The map of

discrimination used in this study to calculate the terrestrial carbon flux from CMDL atmospheric observations [*Ciais et al.*, 1995a] ranges between 18 and 19‰ over the same latitudes. The average discrimination values CCGG inferred from observations are less than the *Ciais et al.* [1995a] model, although about half the sites agree quite well. The data show no meridional gradient in contrast to the *Fung et al.* [1997] result. About half the sites studied also agree reasonably well with the *Lloyd and Farquhar* [1994] model, with the other sites showing higher discrimination. In the CCGG analysis, the origin of the air sampled has not been accounted for, which may explain some of the discrepancy between the models and CCGG calculations.

A Global Data Set for $\delta^{18}O$ of Atmospheric CO_2

The $\delta^{18}O$ of atmospheric CO_2 has great potential as a tool to separate net photosynthetic and respiratory fluxes of CO_2 by land plants. The oxygen of CO_2 can exchange with oxygen in leaf water and in soil water. Because leaf water is typically enriched in ^{18}O relative to ^{16}O due to evaporation of water from leaves, the $\delta^{18}O$ of atmospheric CO_2 that has been in contact with leaf water (the photosynthetic flux) is enriched relative to $\delta^{18}O$ of atmospheric CO_2 that has been in contact with soil water (the respiratory flux). Several papers have recently explored the potential of this tracer technique using GCMs with isotope physics included in the carbon and water cycles [*Yakir et al.*, 1994; *Miller et al.*, 1999; *Peylin et al.*, 1999]. One major hurdle to the further development of this tracer is that air samples collected "wet," that is, when the air is not dried during the sampling process, may experience post-sampling equilibration of oxygen in CO_2 with oxygen in the water vapor in the flask. It was demonstrated that this can occur when air humidities are high [*Gemery et al.*, 1996]. In the past, all flask data for $\delta^{18}O$ of atmospheric CO_2 between the latitude bands of 30°N and 30°S have been flagged as bad. CCGG has known that this approach eliminates some good data but has been unable to discern which samples were good data and which were not. With the addition of several AIRKITs at tropical sites, which are sampling systems that dry air during sampling, data needed to compare sampling systems and generate a data set of $\delta^{18}O$ of atmospheric CO_2 with global coverage are now available. An example of this is shown in Figure 2.8, which compares sampling systems used in parallel at Cape Kumukahi, Hawaii. Note that evacuated flasks compare well with the dried flasks, an important observation because the Pacific Ocean shipboard flasks are evacuated flasks. Multiyear records of $\delta^{18}O$ of atmospheric CO_2 at dried sites also allow assessment of the range of the expected variability in moist, tropical sites and selection of the evacuated and undried data accordingly. The new, filtered data are shown in Figure 2.9 as annual means for each site plotted as a function of latitude.
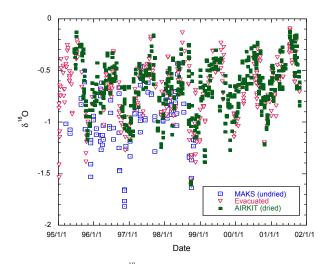
Fig. 2.8. Comparison of $\delta^{18}O$ of atmospheric CO_2 from three different sampling systems at Cape Kumukahi, Hawaii: dried, evacuated, and undried.
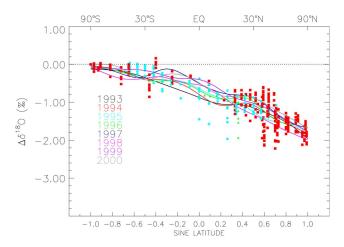

Fig. 2.9. Latitude distribution of $\delta^{18}O$ of atmospheric CO_2 from NOAA data. Annual averages from sites where samples are collected "dry" are shown as solid red squares. Annual averages from the Pacific Ocean and South China Sea shipboard samples collected in 3-L flasks are shown as solid blue circles and green triangles, respectively. The latitude distribution for each year shown is represented by a curve fitted to "dry" records only.